THE IMPACT OF VISCOSITY ON MATERIAL TRANSITIONS IN LARGE FORMAT ADDITIVE MANUFACTURING OF POLYMER COMPOSITES

James C. Brackett[1,*], Elijah P. Charles[2], Matthew B. Charles[2], Tyler C. Smith[3], Vlastimil Kunc[3], Chad E. Duty[1,3]

1 - The Bredesen Center for Interdisciplinary Research, University of Tennessee – Knoxville
Knoxville, TN
2 - Mechanical, Aerospace, and Biomedical Engineering, University of Tennessee – Knoxville
Knoxville, TN
3 - Manufacturing Science Division, Oak Ridge National Laboratory
Oak Ridge, TN

ABSTRACT

The need to produce complex geometries incompatible with traditional manufacturing techniques has fueled rapid growth in Large-Format Additive Manufacturing (LFAM). Printing of polymer composite materials have generated significant interest, but the production of Multi-Material (MM) structures with location-based material properties continues to be a challenge. Extrusion-based techniques have utilized multiple deposition heads to successfully print MM structures with both stiff and flexible regions, but these techniques often result in discrete material boundaries that concentrate stress and act as failure points. To avoid discrete interfaces, a novel dual-hopper configuration was developed for the Big Area Additive Manufacturing (BAAM) system that creates a blended material region within the structure. The ability to blend and freely switch between stiff polymer composites and flexible polymers enables printing of robust MM structures with site-specific properties. This study characterizes the influence of viscosity on a blended material transition between carbon fiber-filled acrylonitrile butadiene styrene (CF-ABS) and unfilled thermoplastic polyurethane (TPU), which have significantly different viscoelastic behaviors

Keywords: 3D Printing, Extrusion, Large-Scale, Multi-Material
Corresponding author: James C. Brackett, jbracke4@vols.utk.edu

1. INTRODUCTION

Additive Manufacturing (AM) offers significant advantages over traditional subtractive manufacturing techniques for producing complex or intricate designs [1, 2]. Substantial interest and investment in the technology has led to rapid growth of the field [3], spawning systems

SAMPE Conference Proceedings. Seattle, WA, April 17-20, 2023. Society for the Advancement of Material and Process Engineering – North America.

DOI: *https://doi.org/10.33599/nasampe/s.23.0166*

compatible with metals [4, 5], ceramics [6, 7], polymers [8-10] and a variety of composites [11, 12]. These diverse systems capitalize on the flexibility of AM to specialize in specific material and production requirements, even within a given field or type of AM. Polymer-based AM, particularly those systems using Extrusion-Deposition Additive Manufacturing (EDAM) techniques, has continued to feature in prototyping and modelling applications in industry but has also become an accessible option for hobbyist activities [13]. However, the production of end-product parts has remained challenging.

1.1 Multiple Materials

Fused Filament Fabrication (FFF) and other EDAM systems were originally designed to utilize a singular material feedstock, limiting their usage in applications requiring multiple materials (MM) throughout the structure. Naturally, many Multi-Material Additive Manufacturing (MMAM) systems, defined as those that do not rely on pre-mixing, pre-compositing, or post-processing techniques to introduce the additional materials [14], have been developed within the last decade to address the need for MM parts. There are many successful examples of MMAM, but the difficulties of bonding layers of different materials have exacerbated the already-present issue of delamination failure in AM parts [15]. Despite several methods for improving bonding in MMAM [16-18], the most common failure modes were consistently delamination at discrete material interfaces, whether between layers or within the same layer. To encourage bonding of dissimilar materials, more recent studies have implemented Functionally Graded Materials (FGM) that distribute the change in materials across multiple discrete regions (stepwise) or a blended region (continuous) instead of a single, sharp switch. Generally, FGM can be classified as either stepwise or continuous but must provide a change in composition, density, or structure in one or more spatial directions [19, 20].

1.1.1 Stepwise FGM

A stepwise FGM utilizes multiple discrete boundaries to create intermediate regions, i.e. steps, and provide a piecewise change in properties in the desired direction(s) [19]. Figure 1A provides a graphical example of a 2-D stepwise FGM. Owing to the success of FGM in improving structural properties, their implementation has been a popular subject in across AM disciplines [21, 22], and numerous EDAM studies have investigated the potential applications of the stepwise approach. One such study demonstrated an improved impact resistance in a stepwise FGM compared to single-material variants using both stiff and flexible materials [23]. Another found an increased delamination resistance at the material boundary by staggering the material boundaries, preventing a single weak-point within the structure [24]. Despite the improvements in performance, these studies and reviews still routinely identify failure-prone material boundaries as the primary challenge [22, 25, 26].

1.1.2 Continuous FGM

The second general classification, continuous FGM are characterized by a non-discrete change in composition, density, or structure throughout the FGM and the absence of discrete material boundaries [19]. Although more difficult to manufacture, the lack of failure-prone discrete boundaries (as illustrated in Figure 1B) provides a significant structural advantage over stepwise FGM. Despite this advantage, MMAM systems capable of printing continuous FGM were uncommon and the result of custom modifications to existing systems rather than commercially

available products. One FFF study was able to find success in developing a unique design that fed two filaments into a single nozzle chamber. The custom FFF instrument was able to first print immiscible thermoplastics as a blended bead through mechanical interlocking [27], which led to a continuous FGM structure created using in-situ blending of the two filaments [28]. Another set of studies also utilized in-situ material blending to incorporate continuous FGM. A step-change in material feedstock was converted into a blended material transition using screw-based EDAM to mix the material boundary during extrusion [8, 29].

Figure 1. Graphical example of a stepwise FGM (A) compared to a continuous FGM (B).

1.2 Large-Format Additive Manufacturing

Another barrier to wide-spread industry adoption of AM has been the speed and scale of production, but within the last few years, multiple Large-Format Additive Manufacturing (LFAM) solutions have been developed. One of the first was the Big Area Additive Manufacturing (BAAM) system, which utilized single screw-based extrusion to print neat and composite polymer thermoplastics and demonstrated significantly faster print speeds and production times [30, 31]. Similar systems have followed in both the commercial space [9] and custom research-oriented equipment [10, 32]. These advances in scale have not been limited to thermoplastic EDAM techniques and have also been successful in thermoset [33] and metal LFAM [4], among others. However, most work with these systems has, again, been limited to single-material production. A notable exception is the BAAM dual-hopper configuration developed to print MM using an LFAM system both within a single layer or across multiple layers [8]. This novel design initiates a step-change in pelletized feedstock from Material A to B then utilizes the in-situ extrusion process to create a blended material transition similar to continuous FGM.

1.3 BAAM Material Transitions

In-situ material switching using the BAAM dual-hopper results in a blended region of continuously changing composition, like that of a continuous FGM, termed the material transition zone. Characterization studies have shown that these transitions were highly repeatable at a given set of processing conditions [29, 34] as well as the potential for control over transition behavior through processing parameters [35], suggesting a process that can be tuned for specific design considerations. Further investigations have also shown that mechanical performance throughout the transition region was dependent primarily on composition, illustrating the benefit of avoiding discrete material boundaries [36]. To identify the most influential processing parameters when printing with the dual-hopper, a comprehensive study using a neat acrylonitrile butadiene styrene

(ABS) and a carbon fiber-filled ABS focused on screw speed, screw geometry, and the effects of switching "to" versus "from" a material (transition direction). The study found that the transition direction had the most significant impact on transition behavior due to a difference in material properties [37]. Considering that the polymer matrix for both materials was ABS, significant differences in material properties were limited. Further, the responsible property must impact flow behavior during extrusion to cause a change in mixing during the transition, which suggests viscoelastic behavior was likely responsible. With literature showing that carbon fiber-filled ABS had significantly higher complex viscosity than the neat resin [38], the change in transition behavior was attributed to that difference in complex viscosities and its effect on flow and mixing during extrusion. This study seeks to further investigate the effect of changing transition direction by increasing the difference in complex viscosities of the two chosen thermoplastics. Since thermoplastic polyurethane (TPU) is typically processed at much lower shear rates and temperatures, material transitions between TPU and a carbon fiber filled ABS were chosen for the investigation. The resulting mismatch in complex viscosities is expected to highlight the importance of transition direction and provide further tools for controlling material transitions printed using the BAAM dual-hopper.

2. EXPERIMENTAL METHODS

The influence of transition direction was investigated by comparing material composition curves printed at various conditions and viscoelastic behavior. Material transitions were printed using the BAAM's dual-hopper configuration [8]. The impact of transition direction and screw rotational speed on the transition behavior was studied by comparing the change in material composition as a function of extruded volume. The relative fractions of TPU and CF-ABS at specified locations throughout each printed transition were determined using Ultrasonic Assisted Digestion (UAD).

2.1 Sample Preparation

Using the BAAM dual-hopper, single-layer material transitions were printed with a neat TPU (RESMART Ultra TPU 70A) and a 20 wt % carbon fiber reinforced ABS (Techmer ES Electrafil ABS 1501 3DP) (CF-ABS) pelletized feedstocks. Pellets were dried for at least 4 hours at 80 °C prior to printing. Bead width, bead height, and nozzle diameter were kept constant for each print at 1.4 cm (0.55 in), 0.51 cm (0.2 in), and 1.02 cm (0.4 in), respectively. The heated print bed (100 °C) and melt (250 °C) temperatures were maintained throughout printing to match standard CF-ABS processing conditions [29]. A custom "mixing" extrusion screw geometry with additional grooves on the shaft in the metering section was used to encourage blending of material boundaries during extrusion. With these print parameters held constant, single-layer material transitions were printed at screw rotational speeds of 100, 200, and 300 RPM. Since each print produced a transition in both the TPU to CF-ABS (T→C) and CF-ABS to TPU (C→T) transition directions (see Figure 2), the three screw speeds and two transition directions resulted in six experimental sets. The beginning of a material transition, i.e. where the dual-hopper switches feedstock, is indicated in Figure 2 by green dots at locations A and C. Similarly, red dots indicate where the BAAM pauses extrusion to move into position for the next transition (B) or concludes the print (D). Printed transitions were labelled and sectioned using a bandsaw for storage. Samples were 1.0 cm long in the print direction and extracted using an Isomet 1000 precision saw and dried for at least 4 hours at 80 °C in preparation for compositional analysis. Pelletized feedstock served as control samples.

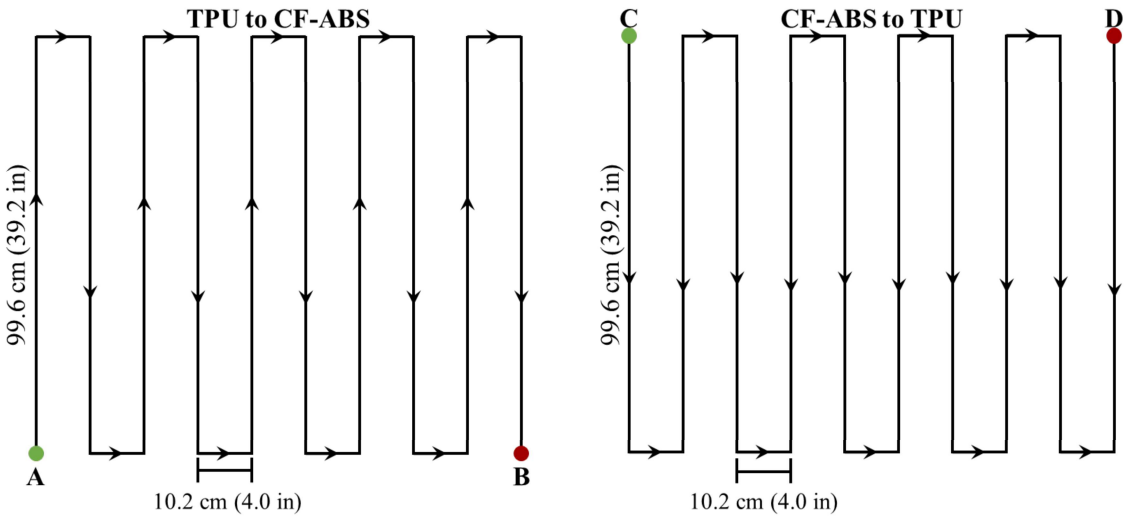

Figure 2. Schematic representation of the path used to print material transition samples.

2.2 Complex Viscosity Measurements

To better understand the compatibility of the flow behaviors when transitioning between CF-ABS and TPU, parallel plate rheology was used to observe the complex viscosity of both materials and quantify the difference in viscoelastic behavior. The complex viscosities, η^*, of both materials and a neat ABS (Techmer ES HIFILL ABS 1512 3DP) for reference were measured using a TA Instruments Discovery Hybrid Rheometer-2 (DHR2) and 25 mm parallel plate geometry. The complex viscosity was measured using an oscillatory frequency sweep from 628 rad/s to 0.1 rad/s with an applied strain of 0.1 % [38, 39]. The frequency sweeps were performed at 250 °C for each material to simulate the typical CF-ABS print conditions that all samples were printed under.

2.3 Compositional Analysis

The fractional amount of each material was determined by measuring the wt % carbon fiber (wt % CF) in the sample, which was obtained using Ultrasonic Assisted Digestion (UAD). Based on ASTM D3171 [40], UAD was developed as an alternative to thermal degradation processes typically used in constituent content analysis of thermoplastic composites. Previous studies have demonstrated the reliability of UAD when using acetone as the solvent [29, 35], but the chemical resistance of TPU inhibited dissolution by acetone. Therefore, Dimethyl Sulfoxide (DMSO) was chosen as a replacement solvent due to the documented vulnerability of TPU [41]. In accordance with the developed UAD procedure, each sample was submerged in 50 mL of DMSO within a sealed test tube and placed in a CPX3800 Ultrasonic Bath. The bath was then heated to 50 °C, and samples were sonicated for at least 10 hours to ensure total dissolution. Using a vacuum filtration system, fully dissolved solutions were filtered through Whatman Grade GF/A glass microfiber filters (47 mm diameter with 1.6 µm pores). The filters were retrieved with minimal disturbance, taking care to preserve the integrity of the captured residue. After dying at 80 °C for at least 4 hours, the combined mass was measured with 0.1 mg resolution using a RADWAG AS 220.R2 Analytical balance. Since carbon fibers were inert in DMSO, the dried sample mass was subtracted from the combined dry mass of solution residue (fibers) and filter to find the dry mass of the fibers alone. The resulting wt % CF was considered representative of material composition and used to

find material percentages by it to 20 wt % CF, as outlined in studies establishing the effectiveness of UAD [29, 35]. These material percentages thus indicated the progression of the material transition.

2.4 Transition Curve Construction

Samples were taken from the material transitions and identified by the travel distance from the hopper switch, d, but the travel distance alone was not an accurate method for comparing the transition behavior. A change in print parameters will change bead shape and, in turn, affect how much material has been extruded at a given d, so a volumetric approach was necessary to accurately represent sample locations. Inconsistent cross-sectional areas, especially in the blended material region, inhibited direct volume measurements, so an indirect approach using volumetric flow rate was used instead. BAAM-specific volumetric flow rates were obtained for both materials at 100, 200, and 300 RPM under the same conditions used when printing samples. Material was first extruded until achieving a steady flow before then pausing extrusion momentarily, translating the print head to the sample site, and resuming extrusion for 30 s. The resulting sample was collected, dried at 80 °C for at least 4 hours, and weighed to obtain material mass, m. Using Equation 1, Q was calculated for each material and rpm combination by multiplying by ρ and dividing by the 30 s extrusion time, t.

$$Q = \frac{m\rho}{t} \quad [1]$$

These flow rates and the measured fractions of TPU (F_{TPU}) and CF-ABS (F_{CF}) obtained using UAD were then used to determine a combined flow rate (Q_R) based on the material composition at that location, as shown in Equation 2.

$$Q_R = F_{CF}Q_{CF} + (1 - F_{CF})Q_{TPU} \quad [2]$$

After calculating the correct flow rate for a given point with Equation 2, the travel distance, d, was converted into volume. The cumulative volume extruded up to the given point, V_E, was found using Equation 3 where Q_R was multiplied by d and divided by gantry travel speed, s.

$$V_E = \frac{Q_R d}{s} \quad [3]$$

Although Equation 3 enabled accurate comparisons of material transitions, it lacked a physical connection to the instrument. Since the functionality of the BAAM dual-hopper ensures that a constant amount of the original material, Material A, will be present in the system when switching to the new feedstock, Material B, there is a limited volume of Material A that can be present in the transition. To maintain conservation of mass, the residual volume of Material A present in the system after switching materials, V_R, represents that finite amount of Material A that can be present in the material transition. While V_R first depended on the internal geometry of the extrusion system, the changing material states from pellets to melt to solid extrudate also affected how the material filled the available space. Therefore, the ratios of bulk (ρ_b) and melt (ρ_m) densities to ρ of Material A were used to determine the volume of Material A occupying the space in the extrusion system. Densities of printed samples were measured using a Quantachrome Helium Pycnometer set to repeat measurements until a standard deviation of less than 0.0005 g/cm^3 was achieved. Bulk

densities, of the pelletized feedstocks were measured using a custom apparatus constructed to match specifications in ASTM D1895 [42]. Specimens were measured five times and averaged. Material melt density was measured in accordance with ASTM D3835 using a Dynisco Laboratory Capillary Rheometer 7001 [43]. Related work presents detailed calculations of V_R using this method and proprietary design drawings [37]. The final step, shown in Equation 4, was normalizing the V_E by V_R and find the normalized volume, V_N.

$$V_N = \frac{V_E}{V_R} \quad [4]$$

Plotting the transitions in terms of V_N provided an important visual and analytical tool: in an "ideal" scenario where the material boundary is maintained throughout extrusion, the change from Material A to B would always occur at $V_N = 1$, or when $V_E = V_R$. As part of the conservation of mass, the area under this curve must be preserved, even in the blended material transitions, because it represents the finite volume of Material A. Any increase or decrease in this area suggests gaining or losing mass, which would not be possible in this closed system. Thus, an intrinsic property of the transition curves is $V_N = 1$ acts as a boundary condition and tool for analyzing the blended region. Any deviation in curve shape when $V_N < 1$ must be mirrored by a cumulatively equal change when $V_N > 1$ to maintain the conservation of mass arising from V_R.

Since only one of the two materials were fiber reinforced, wt % CF was used to represent the change in material composition and plotted against normalized volume. Thresholds of less than 1 wt % CF and greater than 19 wt % CF were considered single-material TPU and CF-ABS, respectively. Figure 3 shows the three distinct zones observed in all transition curves, where L_P indicates the end of the purge zone and L_S indicates the start of the steady state zone. The length of the transition zone is then equal to the difference between the two, as shown in Equation 5. While both the purge and steady-state zones are single-material regions, the transition zone is characterized by a continually changing material composition, in this case carbon fiber content.

$$L_T = L_S - L_P \quad [5]$$

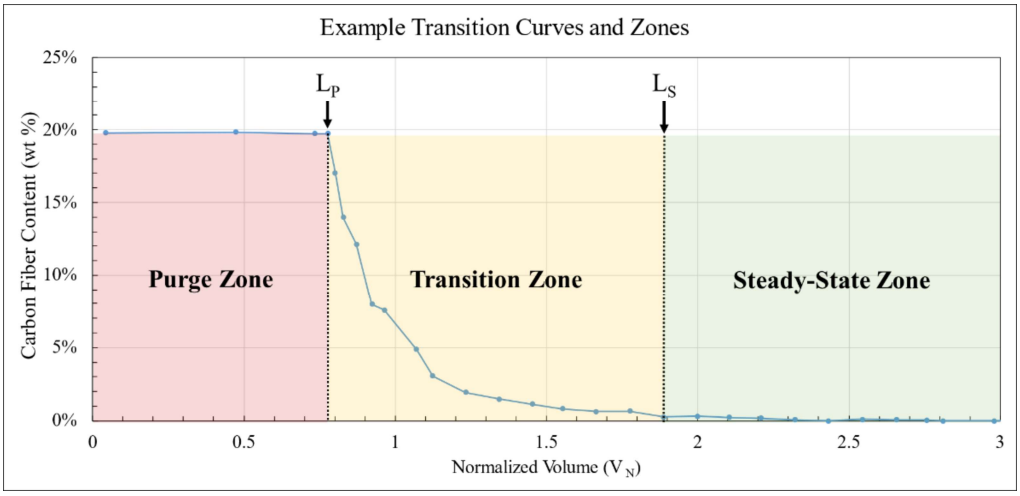

Figure 3. An example transition curve showing the three material transition zones.

3. RESULTS

3.1 Density

Three different densities corresponding to material form were measured for CF-ABS and TPU, and the average values are reported in Table 1. The first, ρ, was the density of the material after deposition onto the print bed whereas ρ_b and ρ_m were the densities of the pelletized feedstock contained in the hopper and the density of the full polymer melt obtained during extrusion. TPU had a higher printed density, which agreed with manufacturer specifications. As a result of the poor packing of the irregularly shaped TPU and cylindrical CF-ABS pellets, the bulk densities were both significantly lower than the material densities. The densities of the polymer melts, however, were nearly identical. The greater decrease in density of TPU relative to CF-ABS was likely due to processing temperatures exceeding those typically used for TPU, which led to an increased susceptibility to shear thinning [44]. As discussed in [37], the ratios of bulk and melt densities to the printed densities were used to find a material-specific V_R for TPU and CF-ABS by relating the material inside to the printed material that could be measured.

Table 1. The average measured densities and standard deviations for both materials.

Material	ρ (g/cm^3)	ρ_b (g/cm^3)	ρ_m (g/cm^3)
CF-ABS	1.099 (0.0004)	0.633 (0.001)	0.894 (0.016)
TPU	1.178 (0.0003)	0.715 (0.005)	0.896 (0.003)

3.2 Viscosity and Flow Rate

The viscoelastic response of TPU, CF-ABS, and a neat ABS were all assessed using parallel plate rheology to investigate shear-thinning behavior and viscosity at the state processing conditions. Figure 4 shows the measured complex viscosities as a function of angular frequency across the studied range. As expected, when comparing a fiber-reinforced thermoplastic to similar neat resins, CF-ABS was significantly more viscous than both the neat ABS and TPU at all frequencies due to fiber-fiber interactions [45]. As in previous work showing that ABS and CF-ABS were always shear-thinning [38, 46], Figure 4 illustrates the shear-thinning behavior of CF-ABS and ABS specimens. Since shear rates seen in BAAM processing were reportedly near 100 s^{-1} [39, 47], the complex viscosities measured at an angular frequency of 628 rad/s were chosen for comparison to TPU. Likely due to the increased temperatures compared to typical processing conditions [44], the complex viscosity of TPU was over an order of magnitude lower than neat ABS at 628 rad/s, indicating that TPU would also have a significantly lower complex viscosity when printing these material transitions. While this figure indicates that TPU exhibited mildly shear thinning and shear-thickening behavior, repeated test observations conclude that the high testing temperature (relative to typical TPU conditions) caused significant discoloration and material ooze at higher shear rates. The resulting loss of material between the parallel plates and likely material degradation suggest that the measured complex viscosity at higher shear rates was artificially inflated. As such, the significant decrease in complex viscosity from ABS to TPU satisfies the criterion required to emphasizing the effect of viscosity on transition.

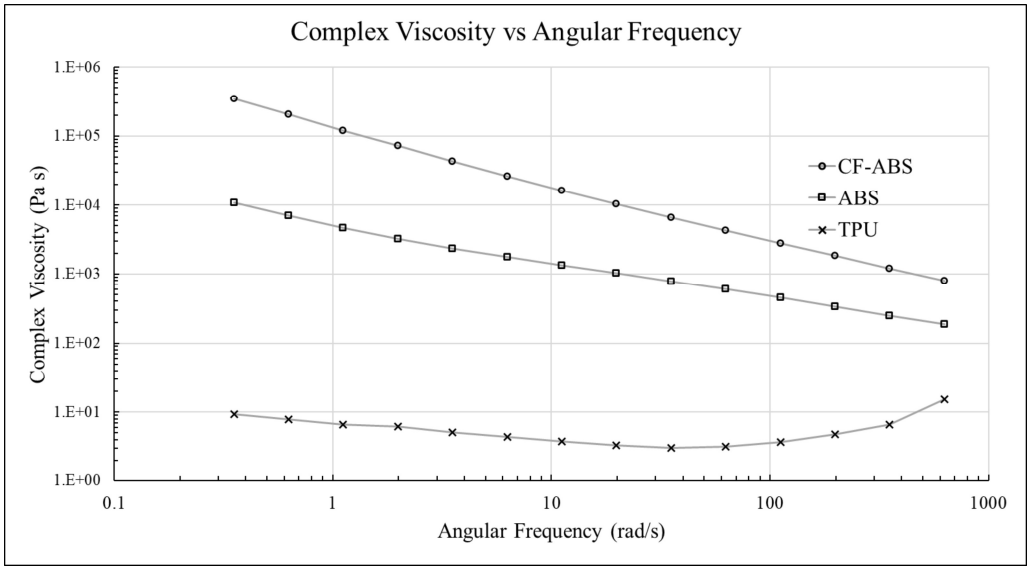

Figure 4. Complex viscosity of CF-ABS, ABS, and TPU as a function of angular frequency.

After confirming a significant difference in complex viscosities, the volumetric flow rates for CF-ABS and TPU were measured and reported in Table 2. As expected, the less viscous TPU exhibited higher volumetric flow rates at each screw speed, but this effect was not constant. Instead, TPU appeared to be more shear-sensitive than CF-ABS at the prescribed processing conditions, leading to significantly higher volumetric flow rates at 200 and 300 RPM.

Table 2. Measured volumetric flow rates at each RPM for both CF-ABS and TPU.

Material	Q_{100} **(cm^3/s)**	Q_{200} **(cm^3/s)**	Q_{300} **(cm^3/s)**
CF-ABS	3.06	5.61	7.46
TPU	3.49	7.73	10.04

3.3 Transition Curve Behavior

Transition curves were created by plotting wt % carbon fiber (wt % CF) as a function of normalized volume. Figure 5 shows the C→T curves for the three examined screw speeds. Each curve exhibits an immediate change in composition at L_P, as expected, followed by a decaying rate of change as the transition approaches steady-state TPU. While the T→C transitions in Figure 6 also exhibit similar behavior at L_P, the rate of change was slower for T→C than C→T. To quantify this difference, the absolute value of the slope at L_P for both 100 RPM curves yielded 0.87 for C→T but only 0.53 for T→C. In addition to the "sharper" change in composition, the C→T curves also have a consistently longer purge zone length. Based on the zone lengths reported in Table 3, the decrease in purge zone length was, on average, 8 % and consistent across screw speeds. These results suggest that there was increased mixing when switching in the T→C direction compared to C→T. Considering that material mixing occurs in the compression and metering zones of the single-screw extruder (SSE), there are two primary competing forces that drive mixing: pressure driven flow and drag flow [48]. This identifies that pressure flow has a significant influence on material mixing while also being dependent on material viscosity. Given the significantly higher viscosity of CF-ABS compared to TPU, it follows that the CF-ABS melt is less influenced by the

competing pressure flow responsible for creating circulation within the melt, which would lead to a reduced mixing of the material boundary. Similarly, the less-viscous TPU is more susceptible to the pressure flow driving it back up the screw, allowing for a relative increase in blending of the material boundary. This interpretation provides an explanation for the influence of transition direction by connecting material viscosity and SSE flow behavior to the dual-hopper material switch.

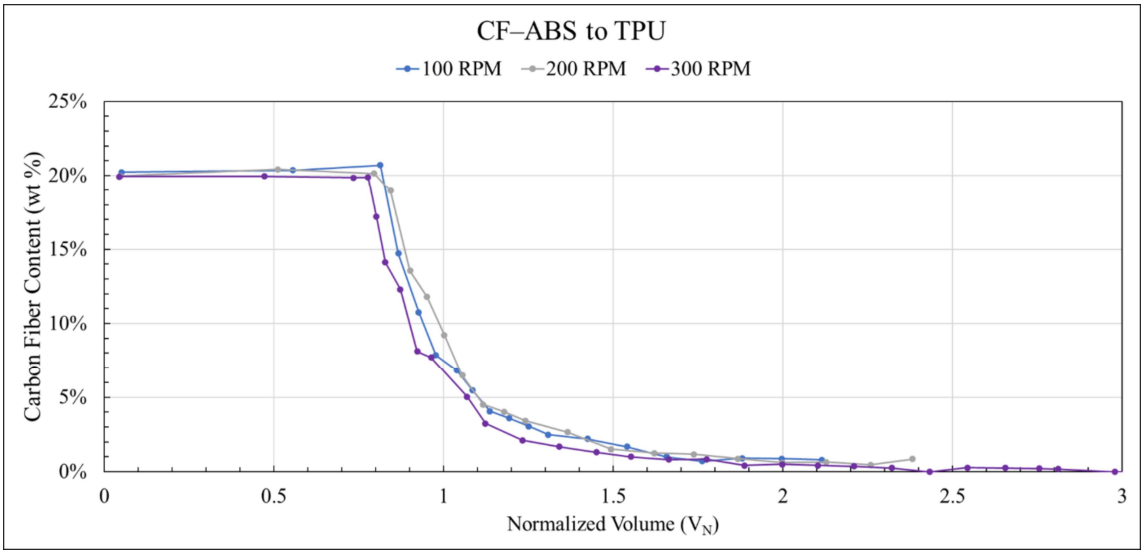

Figure 5. The transition curves for the C→T direction at each studied RPM.

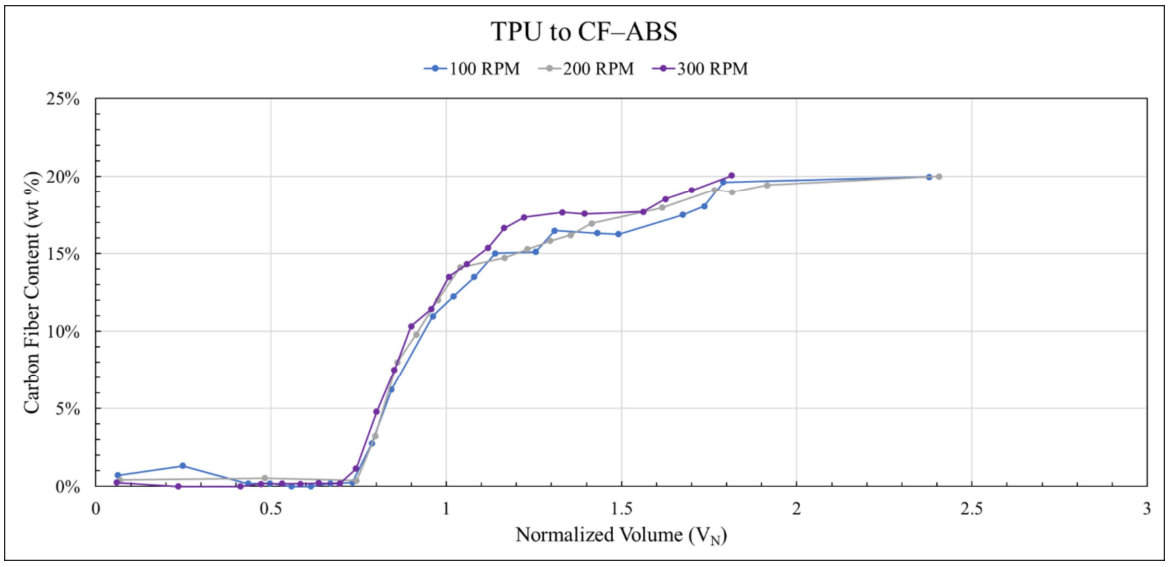

Figure 6. The transition curves in the T→C direction at each studied RPM.

Looking at L_S and using Equation 5 to find the transition zone lengths reported in Table 3 confirms that the studied material transitions do not have a consistent L_T. However, the lengths were consistently longer for T→C than C→T due to the increased mixing, which satisfies the

conservation of mass condition requiring one V_R of Material A be extruded during the transition. Additional consideration shows there were no apparent trends associated with screw speed for any zone length or slope at L_P. Thus, transition direction through material viscosity interactions demonstrated the greatest influence on transition behavior.

Table 3. Transition lengths of the printed specimens.

Direction	Screw Speed (RPM)	Purge Zone (V_N)	Transition Zone (V_N)
CF-ABS to TPU	100	0.81	0.85
	200	0.80	1.07
	300	0.78	0.77
TPU to CF-ABS	100	0.73	1.06
	200	0.74	1.17
	300	0.74	1.07

4. CONCLUSIONS

Multiple material transitions were printed utilizing the novel BAAM dual-hopper configuration. Three different forms of a 20 wt % CF-ABS and a neat TPU were measured to estimate the average material density at various points in the BAAM and calculate a residual volume. The complex viscosities of CF-ABS, ABS, and TPU were measured and reported over a range of angular frequencies. While CF-ABS and ABS were shown to be shear-thinning at the print conditions and agreed with literature, TPU exhibited slight shear-thickening at the shear-profile experienced in the BAAM. Although this was likely due to TPU overflowing the parallel plate geometry, future work will include improved testing and analysis of TPU. The volumetric flow rates of CF-ABS and TPU were measured to use when constructing transition curves. Results suggested TPU was more shear-sensitive than CF-ABS at these processing conditions. Overall, the significant differences in viscoelastic behavior between TPU and CF-ABS justified the material choices for a transition direction study that suspected viscosity was the primary influence on transition behavior.

Material transition curves were constructed using a unique normalized volume approach that included material properties, such as density, in calculations to better isolate processing variables and conditions from convoluting factors. This technique demonstrated that screw speed had a negligible impact on transition behavior. Purge zones were shown to have consistent lengths within a given transition direction where T→C exhibited a shorter average length than C→T due to increased blending of the material boundary during extrusion. Similarly, T→C had a longer average transition zone length than C→T, which agreed with established constraints stating that a reduced amount of Material A prior to $V_N = 1$ must be matched by an equal increase in Material A after $V_N > 1$. By connecting the transition direction, material viscosity, and generalized flow in SSE that is responsible for mixing, this study suggests that material viscosity is the primary factor causing transition direction to have such a noticeable impact. This connection and previous experimental results suggest that material transitions may be tunable by altering the viscosity of the constituent materials. Future work will focus on improving curve resolution with additional measurements to aid development of a predictive model for material transition.

5. ACKNOWLEDGEMENTS

Research sponsored by the U.S. Department of Energy, Office of Energy Efficiency and Renewable Energy, Advanced Manufacturing Office, under contract DE-AC05-00OR22725 with UT-Battelle, LLC. This material was also based upon work supported by the National Science Foundation under Grant No. 2055529 and supported in part by Oak Ridge Institute for Science and Education through the Higher Education Research Experiences Program (HERE). Thanks to Cincinnati Incorporated and Techmer PM for provided material and equipment, and further thanks to the UTK MABE Maker Lab.

6. REFERENCES

[1] Huang, Y., Leu, M. C., Mazumder, J., and Donmez, A. "Additive Manufacturing: Current State, Future Potential, Gaps and Needs, and Recommendations." *Journal of Manufacturing Science and Engineering* 137 (2015), DOI: 10.1115/1.4028725.

[2] Wendel, B., Rietzel, D., Kuhnlein, F., Feulner, R., Hulder, G., and Schmachtenberg, E. "Additive Processing of Polymers." *Macromolecular Materials and Engineering* 293 (2008): 799-809. DOI: 10.1002/mame.200800121.

[3] Alammar, A., Kois, J. C., Revilla-León, M., and Att, W. "Additive Manufacturing Technologies: Current Status and Future Perspectives." *Journal of Prosthodontics* 31 (2022): 4-12. DOI: https://doi.org/10.1111/jopr.13477.

[4] Greer, C., Nycz, A., Noakes, M., Richardson, B., Post, B., Kurfess, T., and Love, L. "Introduction to the Design Rules for Metal Big Area Additive Manufacturing." (in English), *Additive Manufacturing* 27 (2019): 159-166. DOI: 10.1016/j.addma.2019.02.016.

[5] Paolini, A., Kollmannsberger, S., and Rank, E. "Additive Manufacturing in Construction: A Review on Processes, Applications, and Digital Planning Methods." (in English), *Additive Manufacturing* 30 (2019): 13. Art no. 100894, DOI: 10.1016/j.addma.2019.100894.

[6] Clemens, F., Sarraf, F., Borzì, A., Neels, A., and Hadian, A. "Material Extrusion Additive Manufacturing Of advanced Ceramics: Towards the Production of Large Components." *Journal of the European Ceramic Society* (2022), DOI: https://doi.org/10.1016/j.jeurceramsoc.2022.10.019.

[7] Lakhdar, Y., Tuck, C., Binner, J., Terry, A., and Goodridge, R. "Additive Manufacturing of Advanced Ceramic Materials." *Progress in Materials Science* 116 (2021): 100736. DOI: https://doi.org/10.1016/j.pmatsci.2020.100736.

[8] Smith, T., Hassen, A. A., Lind, R., Lindahl, J., Chesser, P., Roschli, A., Kumar, V., Kishore, V., Post, B., Failla, J., Duty, C., Love, L., and Kunc, V. "Dual Material System for Polymer Large Scale Additive Manufacturing." *Society for the Advancement of Material and Process Engineering 2020*. Seattle, WA, June 1, 2020. [Online].

[9] Moreno Nieto, D., Casal López, V., and Molina, S. I. "Large-Format Polymeric Pellet-Based Additive Manufacturing for the Naval Industry." *Additive Manufacturing* 23 (2018): 79-85. DOI: https://doi.org/10.1016/j.addma.2018.07.012.

[10] Cosson, B., Akué Asséko, A. C., Pelzer, L., and Hopmann, C. "Radiative Thermal Effects in Large Scale Additive Manufacturing of Polymers: Numerical and Experimental Investigations." *Materials* 15 (2022): 1052. [Online]. Available: https://www.mdpi.com/1996-1944/15/3/1052.

[11] Yan, S. Q., Chen, L., Yob, A., Renshaw, D., Yang, K., Givord, M., and Liang, D. "Multifunctional Metal Matrix Composites by Friction Stir Additive Manufacturing." (in English), *Journal of Materials Engineering and Performance* 31 (2022): 6183-6195. DOI: 10.1007/s11665-022-07114-7.

[12] van de Werken, N., Tekinalp, H., Khanbolouki, P., Ozcan, S., Williams, A., and Tehrani, M. "Additively Manufactured Carbon Fiber-Reinforced Composites: State of the Art and Perspective." (in English), *Additive Manufacturing* 31 (2020): 19. Art no. 100962, DOI: 10.1016/j.addma.2019.100962.

[13] Altıparmak, S. C., Yardley, V. A., Shi, Z., and Lin, J. "Extrusion-Based Additive Manufacturing Technologies: State of the Art and Future Perspectives." *Journal of Manufacturing Processes* 83 (2022): 607-636. DOI: https://doi.org/10.1016/j.jmapro.2022.09.032.

[14] Vaezi, M., Chianrabutra, S., Mellor, B., and Yang, S. "Multiple Material Additive Manufacturing – Part 1: A Review." *Virtual & Physical Prototyping* 8 (2013): 19-50. DOI: 10.1080/17452759.2013.778175.

[15] Bandyopadhyay, A.Heer, B. "Additive Manufacturing of Multi-Material Structures." *Materials Science and Engineering: R: Reports* 129 (2018): 1-16. DOI: https://doi.org/10.1016/j.mser.2018.04.001.

[16] Issayev, G., Aitmaganbet , A., Shehab, E., and Ali, H. "Bonding Strength Analysis of Multi-Material and Multi-Color Specimens Printed with Multi-Extrusion Printer." *Manufacturing Technology Journal* 21 (2021): 627-633. DOI: 10.21062/mft.2021.072.

[17] Lopes, L. R., Silva, A. F., and Carneiro, O. S. "Multi-Material 3d Printing: The Relevance of Materials Affinity on the Boundary Interface Performance." *Additive Manufacturing* 23 (2018): 45-52. DOI: https://doi.org/10.1016/j.addma.2018.06.027.

[18] Ali, M. H., Mir-Nasiri, N., and Ko, W. L. "Multi-Nozzle Extrusion System for 3d Printer and Its Control Mechanism." (in English), *International Journal of Advanced Manufacturing Technology* 86 (2016): 999-1010. DOI: 10.1007/s00170-015-8205-9.

[19] Udupa, G., Rao, S. S., and Gangadharan, K. V., "Functionally Graded Composite Materials: An Overview," in *International Conference on Advances in Manufacturing and Materials Engineering*, vol. 5, S. Narendranath, M. R. Ramesh, D. Chakradhar, M. Doddamani, and S. Bontha Eds., (Procedia Materials Science. Amsterdam: Elsevier Science Bv, 2014, pp. 1291-1299.

[20] Mahamood, R. M.Akinlabi, E. T., "Types of Functionally Graded Materials and Their Areas of Application," in *Functionally Graded Materials*. Cham: Springer International Publishing, 2017, pp. 9-21.

[21] Yan, L., Chen, Y., and Liou, F. "Additive Manufacturing of Functionally Graded Metallic Materials Using Laser Metal Deposition." *Additive Manufacturing* 31 (2020): 100901. DOI: https://doi.org/10.1016/j.addma.2019.100901.

[22] Loh, G. H., Pei, E., Harrison, D., and Monzón, M. D. "An Overview of Functionally Graded Additive Manufacturing." *Additive Manufacturing* 23 (2018): 34-44. DOI: https://doi.org/10.1016/j.addma.2018.06.023.

[23] Bartlett, N. W., Tolley, M. T., Overvelde, J. T. B., Weaver, J. C., Mosadegh, B., Bertoldi, K., Whitesides, G. M., and Wood, R. J. "A 3d-Printed, Functionally Graded Soft Robot Powered by Combustion." (in English), *Science* 349 (2015): 161-165. DOI: 10.1126/science.aab0129.

[24] Vu, I. Q., Bass, L. B., Williams, C. B., and Dillard, D. A. "Characterizing the Effect of Print Orientation on Interface Integrity of Multi-Material Jetting Additive Manufacturing." *Additive Manufacturing* 22 (2018): 447-461. DOI: https://doi.org/10.1016/j.addma.2018.05.036.

[25] Pajonk, A., Prieto, A., Blum, U., and Knaack, U. "Multi-Material Additive Manufacturing in Architecture and Construction: A Review." *Journal of Building Engineering* 45 (2022): 103603. DOI: https://doi.org/10.1016/j.jobe.2021.103603.

[26] Hasanov, S., Alkunte, S., Rajeshirke, M., Gupta, A., Huseynov, O., Fidan, I., Alifui-Segbaya, F., and Rennie, A. "Review on Additive Manufacturing of Multi-Material Parts: Progress and Challenges." *Journal of Manufacturing and Materials Processing* 6 (2022): 4. [Online]. Available: https://www.mdpi.com/2504-4494/6/1/4.

[27] Khondoker, M. A. H., Asad, A., and Sameoto, D. "Printing with Mechanically Interlocked Extrudates Using a Custom Bi-Extruder for Fused Deposition Modelling." *Rapid Prototyping Journal* 24 (2018): 921-934. DOI: 10.1108/RPJ-03-2017-0046.

[28] Khondoker, M. A., Baheri, N., and Sameoto, D. "Tendon-Driven Functionally Gradient Soft Robotic Gripper 3d Printed with Intermixed Extrudate of Hard and Soft Thermoplastics." (in English), *3d Printing and Additive Manufacturing* 6 (2019): 191-203. DOI: 10.1089/3dp.2018.0102.

[29] Brackett, J., Yan, Y., Cauthen, D., Kishore, V., Lindahl, J., Smith, T., Sudbury, Z., Ning, H., Kunc, V., and Duty, C. "Characterizing Material Transitions in Large-Scale Additive Manufacturing." *Additive Manufacturing* 38 (2021): 101750. DOI: https://doi.org/10.1016/j.addma.2020.101750.

[30] Duty, C. E.Love, L. J., "Cincinnati Big Area Additive Manufacturing (Baam)," United States, 2015-03-04 2015. [Online]. Available: https://www.osti.gov/biblio/1210140 https://www.osti.gov/servlets/purl/1210140

[31] Love, L. J., Kunc, V., Rios, O., Duty, C. E., Elliott, A. M., Post, B. K., Smith, R. J., and Blue, C. A. "The Importance of Carbon Fiber to Polymer Additive Manufacturing." *Journal of Materials Research* 29 (2014): 1893-1898. DOI: 10.1557/jmr.2014.212.

[32] Gawali, S. K., Pandey, G. C., Bajpai, A., and Jain, P. K. "Large-Part Manufacturing Using Cnc-Assisted Material Extrusion-Based Additive Manufacturing: Issues and Challenges." *International Journal on Interactive Design and Manufacturing (IJIDeM)* (2022), DOI: 10.1007/s12008-022-01097-4.

[33] Romberg, S. K., Hershey, C. J., Lindahl, J. M., Carter, W. G., Condon, J., Kunc, V., and Compton, B. G. "Large-Scale Reactive Thermoset Printing: Complex Interactions between Temperature Evolution, Viscosity, and Cure Shrinkage." (in English), *International Journal of Advanced Manufacturing Technology* 123 (2022): 3079-3094. DOI: 10.1007/s00170-022-10380-3.

[34] Brackett, J., Yan, Y., Cauthen, D., Kishore, V., Lindahl, J., Smith, T., Ning, H., Kunc, V., and Duty, C. "Development of Functionally Graded Material Capabilities in Large-Scale Extrusion Deposition Additive Manufacturing." *Solid Freeform Fabrication Symposium*. Austin, TX, 2019. pp. 1793-1803, doi: http://dx.doi.org/10.26153/tsw/17437.

[35] Brackett, J., Cauthen, D., Smith, T., Kunc, V., and Duty, C. "The Influence of Processing Parameters on the Transition Zone for Blended Material 3d Printing." *SAMPE 2020 Virtual Series | Additive Manufacturing*. Seattle, WA, June 1, 2020. [Online].

[36] Brackett, J., DeFilippis, A., Smith, T., Hassen, A. A., Kunc, V., and Duty Chad, E. "Evaluating the Mechanical Properties within the Transition Region of Multi-Material

Large-Format Extrusion Additive Manufacturing." *Solid Freeform Fabrication Symposium*. Austin, TX, November 4, 2022. pp. 1210-1222.

[37] Brackett, J., Charles, E., Cauthen, D., Smith, T., Kishore, V., Kunc, V., and Duty Chad, E. "The Impact of Processing Parameters on the Transition Behavior of Blended Material Large Format Additive Manufacturing." *In Preparation* (2023).

[38] Walker, R., Helton, C., Kunc, V., and Duty, C. "Rheological Evaluation of Printability for Recycled Carbon Fiber Acrylonitrile Butadiene Styrene." *SAMPE 2022*. Charlotte, May 23-26, 2022. Society for the Advancement of Material and Process Engineering - North America. p. 10, doi: 10.33599/nasampe/s.22.0777.

[39] Duty, C., Ajinjeru, C., Kishore, V., Compton, B., Hmeidat, N., Chen, X., Liu, P., Hassen, A. A., Lindahl, J., and Kunc, V. "What Makes a Material Printable? A Viscoelastic Model for Extrusion-Based 3d Printing of Polymers." *Journal of Manufacturing Processes* 35 (2018): 526-537. DOI: https://doi.org/10.1016/j.jmapro.2018.08.008.

[40] ASTM Standard D3171-15, 2015, "Standard Test Methods for Constituent Content of Composite Materials" ASTM International, West Conshohocken, PA, 2015, DOI: 10.1520/D3171-15, https://www.astm.org/d3171-15.html.

[41] Mi, H.-Y., Jing, X., Salick, M. R., Cordie, T. M., and Turng, L.-S. "Carbon Nanotube (Cnt) and Nanofibrillated Cellulose (Nfc) Reinforcement Effect on Thermoplastic Polyurethane (Tpu) Scaffolds Fabricated Via Phase Separation Using Dimethyl Sulfoxide (Dmso) as Solvent." *Journal of the Mechanical Behavior of Biomedical Materials* 62 (2016): 417-427. DOI: https://doi.org/10.1016/j.jmbbm.2016.05.026.

[42] ASTM Standard D1895-17, 2017, "Standard Test Methods for Apparent Density, Bulk Factor, and Pourability of Plastic Materials" ASTM International, West Conshohocken, PA, 2017, DOI: 10.1520/D1895-17,

[43] ASTM Standard D3835-16, 2016, "Stnadard Test Method for Determination of Polymeric Materials by Means of a Capillary Rheometer" ASTM International, West Conshohocken, PA, 2016, DOI: 10.1520/D3835-16,

[44] Rauwendaal, C., "6 - Important Polymer Properties," in *Polymer Extrusion (Fifth Edition)*, C. Rauwendaal Ed., 5th ed.: Hanser, 2014, ch. 6, pp. 191-253.

[45] Kotsilkova, R., "Dynamic Rheological Properties of Glass Fiber Suspensions," in *Theoretical and Applied Rheology*, P. Moldenaers and R. Keunings Eds. Amsterdam: Elsevier, 1992, pp. 856-858.

[46] Ajinjeru, C., "Rheological Evaluation and Guidelines of High-Performance Amorphous Thermoplastics and Carbon Fiber Reinforced Composites for Additive Manufacturing," University of Tennessee, 2020.

[47] Ajinjeru, C., Kishore, V., Chen, X., Lindahl, J., Sudbury, Z., Hassen, A. A., Kunc, V., Post, B., Lonnie, L., and Duty, C. E. "The Influence of Rheology on Melt Processing Conditions of Amorphous Thermoplastics for Big Area Additive Manufacturing (Baam)." *Solid Freeform Fabrication Symposium*. Austin, TX, 2016. p. 8.

[48] Rauwendaal, C., "5 - Fundamental Principles," in *Polymer Extrusion (Fifth Edition)*, C. Rauwendaal Ed., 5th ed.: Hanser, 2014, ch. 5, pp. 147-189.